

THE INFRARED DETECTION OF THE PULSAR WIND NEBULA IN THE GALACTIC SUPERNOVA REMNANT 3C 58

P. SLANE¹, D. J. HELFAND², S. P. REYNOLDS³, B. M. GAENSLER⁴, A. LEMIERE¹, AND Z. WANG⁵

To Appear in ApJ Letters

ABSTRACT

We present infrared observations of 3C 58 with the *Spitzer Space Telescope* and the Canada-France-Hawaii Telescope. Using the IRAC camera, we have imaged the entire source resulting in clear detections of the nebula at 3.6 and 4.5 μm . The derived flux values are consistent with extrapolation of the X-ray spectrum to the infrared band, demonstrating that any cooling break in the synchrotron spectrum must occur near the soft X-ray band. We also detect the torus surrounding PSR J0205+6449, the 65 ms pulsar that powers 3C 58. The torus spectrum requires a break between the infrared and X-ray bands, and perhaps multiple breaks. This complex spectrum, which is an imprint of the particles injected into the nebula, has considerable consequences for the evolution of the broadband spectrum of 3C 58. We illustrate these effects and discuss the impact of these observations on the modeling of broadband spectra of pulsar wind nebulae.

Subject headings: ISM: individual (3C 58) — pulsars: general — pulsars: individual (PSR J0205+6449) — supernova remnants

1. INTRODUCTION

3C 58 is a flat-spectrum radio nebula ($\alpha \approx 0.1$, where $S_\nu \propto \nu^{-\alpha}$) for which upper limits based on *IRAS* observations indicate a spectral break between the radio and infrared bands (Green & Scheuer 1992). X-ray observations reveal a nonthermal spectrum from the nebula, with an average photon index $\Gamma = \alpha + 1 \sim 2.3$ (Torii et al. 2000) that varies with radius, becoming steeper toward the outer regions of the nebula (Slane et al. 2004; hereafter S04). Subsequent observations with the *Chandra X-ray Observatory* discovered PSR J0205+6449 (Murray et al. 2002), the central pulsar in 3C 58 and one of the most energetic pulsars known in the Galaxy, with a spin-down luminosity $\dot{E} = 2.7 \times 10^{37}$ ergs s^{-1} . The pulsar powers a faint jet and is surrounded by a toroidal structure apparently associated with flows just downstream of the pulsar wind termination shock (S04). The outskirts of the pulsar wind nebula (PWN) reveal faint thermal emission associated with ejecta and/or ambient material swept up by 3C 58 (Bocchino et al. 2001; S04; Gotthelf et al. 2006).

3C 58 has often been associated with SN 1181 (Stephenson & Green 2005). However, the low break frequency would then suggest an unphysically large magnetic field ($> 2.5\text{mG}$) if interpreted as the result of synchrotron losses. More recent investigations of the dynamics of the system (Chevalier 2005), the radio expansion rate (Bietenholz 2006), and the velocity of optical filaments (Rudie & Fesen 2007) argue convincingly that the age of the system is more like ~ 2500 years – a value closer to the characteristic age of PSR J0205+6449 ($\tau_c = 5.38 \times 10^3$ yr; Murray et al. 2002) – but even at this age the magnetic field in a synchrotron-loss scenario would be uncomfortably large and inconsistent with the fact that the nonthermal X-ray emission extends all the way to the radio

boundary of the PWN (S04). This discrepancy has prompted a number of explanations: 1) the pulsar in 3C 58 underwent a rapid decline in its output at some early epoch (Green & Scheuer 1992); 2) the radiation spectrum reflects structure in the spectrum of magnetic turbulence in the nebula (Fleishman & Bietenholz 2007); and 3) the low-frequency break is inherent in the injection spectrum from the pulsar (Frail 1998).

The radial steepening of the X-ray spectrum in 3C 58, while indicative of synchrotron losses, is also difficult to understand in detail. Assuming a power-law injection of particles into the nebula, the spectral index varies with radius much more slowly than models for an adiabatically-expanding nebula would predict (Reynolds 2003). This problem of a low-frequency spectral break and a spectral index that steepens slowly with radius is found in several other PWNe as well, including G21.5–0.9 (Woltjer et al. 1997, Slane et al. 2000), making a more detailed investigation of the broadband spectra of these nebulae important.

Here we report on observations of 3C 58 with the *Spitzer Space Telescope* (*SST*) and Canada-France-Hawaii Telescope (*CFHT*). In §2 we describe the observations and the data reduction procedures. In §3 we discuss the analysis of these data. A discussion and interpretation of the broadband spectrum of 3C 58 is presented (§4) followed by our conclusions in (§5).

2. OBSERVATIONS AND DATA REDUCTION

3C 58 was observed by the *SST* on 18 January 2005 (Program ID 3647) using the Infrared Array Camera (IRAC). A complete mapping was carried out using a 54-position dither with the full array readout, using both fields of view so as to obtain full coverage of the PWN as well as a background region at all four wavelengths. We used 100 s frametimes, yielding a minimum exposure of 1200 s in the outer regions of the nebula, with increasing overlap in the center leading to as much as 5400 s of total integration time.

The IRAC data were processed and mosaiced using standard pipelines. Images were obtained at 3.6, 4.5, 5.8, and 8 μm . Our images reveal emission from 3C 58 in both the 3.6 and 4.5 μm bands. The nebula is not seen above the very high foreground/background emission at 5.8 and 8 μm . In Figure 1 we present the VLA image of 3C 58 (Reynolds &

¹ Harvard-Smithsonian Center for Astrophysics, 60 Garden Street, Cambridge, MA 02138.

² Columbia Astrophysics Laboratory, Columbia University, 550 West 120th Street, New York, NY 10027.

³ Department of Physics, North Carolina State University, Box 8202, Raleigh, NC 27695-8202.

⁴ School of Physics A29, The University of Sydney, NSW 2006, Australia.

⁵ Department of Physics, McGill University, 3600 University Street, Montreal, QC H3A 2T8, Canada.

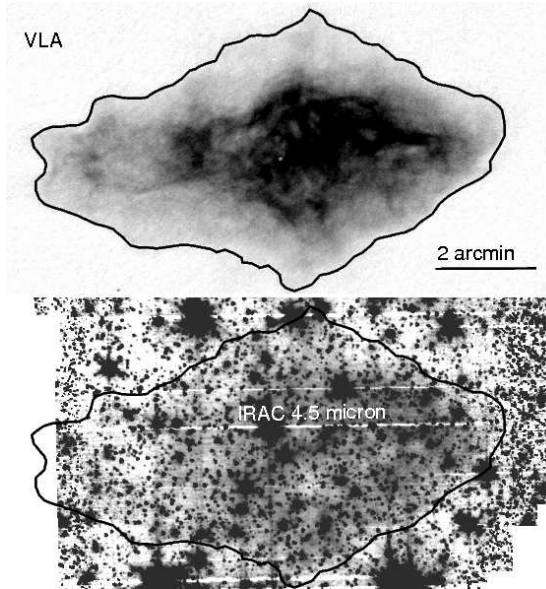


FIG. 1.— VLA and IRAC images of 3C58. The outermost radio contour is shown on the IRAC ($4.5 \mu\text{m}$) image, where the PWN is clearly detected.

Aller 1985) along with the $4.5 \mu\text{m}$ image, with a single contour representing the outer boundary of the radio emission. The PWN is clearly detected, with the infrared (IR) emission extending all the way to the radio boundary in regions of the highest signal-to-noise. The nebula is not detected at longer IRAC wavelengths where PAH emission from Galactic dust dominates the field.

While the emission in the shorter wavelength bands is severely contaminated by stars, the overall morphology is clearly seen, and the flux can be determined to within a factor of a few by scaling the emission from numerous star-free regions, spread across the PWN, to the entire size of the nebula. The overall morphology of the IR emission from 3C 58 is strikingly similar to that seen in the radio and X-ray bands (S04). The emission extends all the way to the radio boundaries, indicating that no synchrotron loss breaks occur at longer wavelengths. Some regions of enhanced or diminished emission match well with those seen in the other bands (notably the large cavity on the eastern side), suggesting that we are observing primarily synchrotron radiation, although we cannot yet rule out a component associated with shock-heated dust. The derived flux does not demand a change in the spectrum between the IR and X-ray bands, although the uncertainties could accommodate a modest spectral break.

Chandra observations of 3C 58 reveal a central pulsar surrounded by an extended torus (Slane et al. 2002). In Figure 2, we show the *Chandra* image of the pulsar, torus, and jet (left) alongside the IRAC $8 \mu\text{m}$ image of the same region. Remarkably, the IRAC image reveals emission from the torus surrounding the pulsar. The source is extended on the same spatial scales and is seen in all four IRAC bands. We have also obtained a *J*-band image of this region from the Canadian Astronomy Data Center. The image was made on 2002 August 16 with the KIR near-IR camera at the Canada-France-Hawaii Telescope. The torus emission observed in IRAC is not detected in the *J* image, in contrast with eight faint stars in the field which are detected in both the *J* and $3.6 \mu\text{m}$ images, confirming that the extended emission has non-stellar colors. The IRAC observations represent only the second detection of a pulsar torus in the IR band (the first being in the Crab Neb-

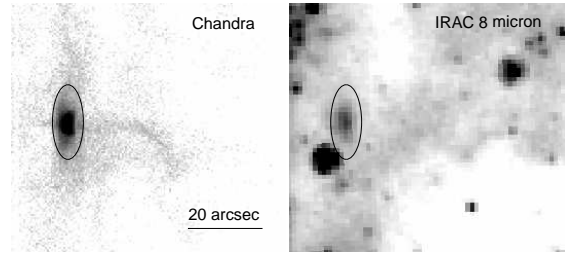


FIG. 2.— *Chandra* image of PSR J0205+6449 in 3C58, and its associated torus (indicated by the ellipse) and jet (left) and the IRAC $8 \mu\text{m}$ image of the same region (right). The torus is clearly detected here as well as in the other three IRAC bands.

ula – Temim et al. 2006), providing new constraints on the evolution of the particles as they flow from the termination shock into the PWN (see Section 4). There is no convincing evidence for emission from the pulsar jet.

3. ANALYSIS AND INTERPRETATION

We derived flux measurements for 3C 58 and its pulsar torus in each of the IRAC bands. For the entire nebula, the diffuse emission is heavily contaminated by stars (Figure 1). Our flux estimates are thus scaled values based on measurements in small star-free regions. Because the brightness of the diffuse emission is nonuniform, the uncertainty on the scaled flux is large. Moreover, the background level also varies considerably across the field. We have thus repeated the measurements using several different background regions. The quoted uncertainties are thus dominated by systematic uncertainties which we estimate at $\sim 40\%$. Flux values for the detected regions are listed in Table 1, where we have corrected the observed flux values using extinction corrections from Indebetouw et al. (2005). As indicated in Figure 3, where we have plotted the spectrum of 3C 58 from the radio band through the X-ray band, the flux values measured by IRAC are consistent with the extrapolation of the X-ray spectrum to the mid-IR band.

The morphology of the IR emission from 3C 58 is very similar to that seen in the radio band, suggesting a synchrotron origin. In particular, there is a good correspondence between discrete radio filaments and enhanced emission in the IRAC images. Optical filaments in 3C 58 (van den Bergh 1978; S04; Rudie & Fesen 2007), which presumably originate from ambient gas overtaken by the expansion of the PWN, do not show a good spatial correspondence with the radio or IR structures, suggesting that the IR emission is not dominated by dust or line contributions. This is similar to the results from *Spitzer* observations of the Crab Nebula (Temim et al. 2006), where emission in the IRAC band is also identified primarily with synchrotron radiation.

For the pulsar torus, we have extracted the flux from a small ellipse centered on the source, oriented north-south with semi-major and minor axes of 7.8 and 4.9 arcsec (slightly smaller than that shown in Figure 2), using a circular background region of radius 12.7 arcsec, centered on the torus, with regions including the torus as well as faint stars removed. To determine the flux uncertainties, we repeated the procedure using several different background regions; we quote the difference between the highest and lowest flux determinations using these background estimates. The flux values are presented in Table 1, and are plotted in Figure 3 along with the X-ray spectrum (S04). The radio upper limit was determined from a 1.4 GHz VLA image (Reynolds & Aller 1985) by adding to this image an elliptical gaussian centered on the pulsar (with dimensions $28.0'' \times 7.9''$, and with the long axis oriented north-

TABLE 1
IRAC FLUX DENSITIES

Region	3.6 μm	4.5 μm	5.8 μm	8 μm
PWN ^a	2.8 ± 1.2	7.1 ± 2.8	—	—
Torus ^b	1.2 ± 0.6	1.6 ± 0.8	2.3 ± 1.2	3.4 ± 1.7

NOTE. — All flux densities are extinction-corrected. Dashes indicate non-detections. Quoted errors correspond to systematic uncertainties.

a) Flux in units of 10^{-2} Jy
b) Flux in units of 10^{-4} Jy

south, as indicated in the *Chandra* image) and steadily increasing the flux until the simulated source was readily detectable above the emission from the nebula. The IRAC data for the torus require a break in the spectrum between the X-ray and IR bands.

There is little question that torus emission is synchrotron in nature; there is insufficient dust in the environment of the pulsar termination shock to provide a shocked dust component to the emission. We do not detect the pulsar jet (seen in X-rays – Figure 2) in the IRAC images, but this does not provide a significant constraint; scaling L_{IR}/L_x from the torus to the jet yields a predicted IR flux that is well below the background levels in the IRAC images.

4. DISCUSSION

The broadband spectra of 3C 58 and its torus, shown in Figure 3, display several distinct features. The overall spectrum from the PWN appears to have two steepening breaks, one just beyond the radio band and another somewhere in the IR band (indicated by dotted and dashed lines). The torus spectrum also requires at least one steepening break between the IR and X-ray bands (dashed line) – a conclusion that has considerable consequences for modeling of the PWN spectrum. If the spectral index of the torus matches that of the PWN in the radio band (see discussion below), the situation is even more complicated; the torus spectrum then needs a steepening break between the radio and IR bands as well as two breaks (one steepening and one flattening) between the IR and X-ray bands (dotted lines).

The broadband spectrum of a PWN reflects both intrinsic and evolutionary effects. Some distribution of particles leaves the pulsar light cylinder, and may evolve before reaching the termination shock where it is thermalized and further modified. Subsequent evolution in the expanding nebula, including diffusion, convection, and energy losses in the evolving nebular magnetic field, all affect the integrated spectrum we observe. For a power-law injection of particles from the pulsar, a constant magnetic field in the nebula yields a power law synchrotron spectrum with a break at a frequency $\nu_b \approx 10^{21} B_{\mu\text{G}}^{-3} t_3^{-2}$ Hz (where $B_{\mu\text{G}}$ is the magnetic field strength, in μG , and t_3 is the age in units of 10^3 yr) above which the synchrotron cooling time of the radiating particles is less than the age of the nebula. For an injection spectrum $\frac{dN}{dE} = AE^{-s}$ where N is the number of particles and A is the normalization, the radiated spectrum is $S_\nu \propto \nu^{-\alpha}$ where $\alpha = (s-1)/2$ for $\nu < \nu_b$ and $\alpha = s/2$ for $\nu > \nu_b$.

The integrated spectrum of a PWN is, in fact, much more complicated than a simple power law with a sharp synchrotron break (e.g., Reynolds & Chevalier 1984). Indeed, spectral breaks with $\Delta\alpha$ different from 0.5 are possible in inhomogeneous models (e.g. Kennel & Coroniti 1984, Reynolds &

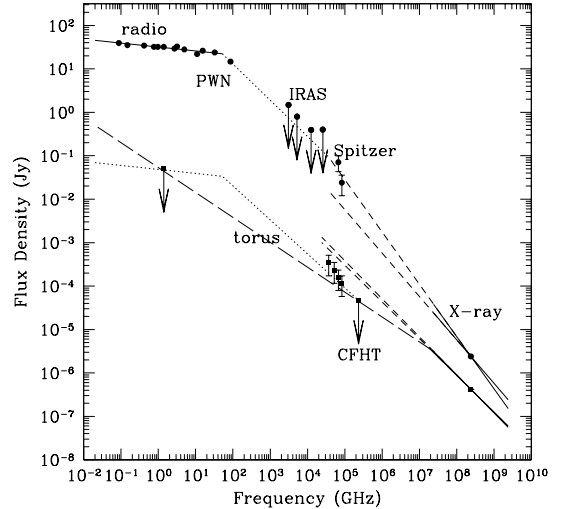


FIG. 3.— The flux of all of 3C 58 (upper) and its torus (lower), plotted from the radio to the X-ray band. While the torus is not detected in the radio band, the IRAC data requires a flattening of the X-ray spectrum when extrapolated back to the longer wavelength band.

Chevalier 1984), and are often observed in PWNe. Variations in the magnetic field with time, to be expected as the PWN expands, can also result in a broadening of the synchrotron break region. In addition, the decline of the pulsar input power with time results in modification of the photon spectrum with time. Electron energies evolve due both to adiabatic losses (where E scales inversely as the mean PWN radius), and due to synchrotron losses (where electrons with energies above an evolving cutoff energy all move to just below that energy). Fossil or intrinsic breaks below the synchrotron break energy will therefore evolve differently with time than the synchrotron break frequency, while breaks above the synchrotron break frequency will tend to be eliminated by synchrotron losses. As the PWN expands and the mean magnetic field weakens, the synchrotron-loss break will move up in frequency, while any fossil breaks should move down (Woltjer et al. 1997). The broadband spectrum thus contains indications of the nebula age, the pulsar input spectrum, and its evolution.

While a complete modeling of the broadband spectrum of 3C 58, including the effects of (asymmetric) adiabatic expansion, is beyond the scope of this Letter, it is instructive to illustrate the effects of a break in the particle injection spectrum. In Figure 4, we plot synchrotron spectra for an evolving population of electrons assuming two different forms for the electron spectrum injected into a uniform magnetic field. In panel (a), we show the electron spectrum for a power law injection, while panel (b) shows a broken power law electron spectrum with a break energy at 60 GeV and indices of 1.1 and 3.3 below and above this break. The magnetic field is $B = 10 \mu\text{G}$, and the upper energy limit on the electron energy is set by the condition that the electron gyroradius not exceed the termination shock radius in 3C 58, $r_{ts} \approx 0.2$ pc assuming a distance of 3.2 kpc. The lower limit on the particle energy is determined by the condition that the integrated electron energy not exceed $\frac{1}{1+\sigma} \dot{E} t$, where \dot{E} is the measured spin-down loss rate for PSR J0205+6449, t is the assumed age (see below), and $\sigma = 0.001$ is the assumed magnetization parameter of the wind. In each case, the dashed curve corresponds to the spectrum at the time of injection (integrated over 50 years)

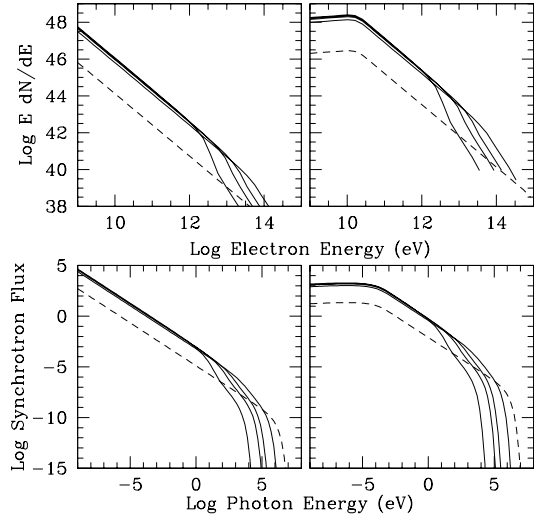


FIG. 4.— Simulated spectra for synchrotron emission from electrons in a PWN. Upper panels show electron spectra for a power law input (a) and a broken power law input (b), while panels (c) and (d) show the associated synchrotron emission. Dashed curves correspond to the injected particles (integrated over 50 years), and solid curves represent the accumulation of the particles (and associated emission) after 1000, 2000, 3000, and 6000 years (from left to right). See text for description.

and the solid curves correspond to the built-up population after a period of 1000, 2000, 3000, and 6000 years. The spectral break at high energies is the result of synchrotron losses.

In panels (c) and (d) we plot the associated synchrotron spectra for these electron populations. It is evident that the injection break in electron spectrum produces a low-energy break in the synchrotron spectrum whose break energy is constant in time, while the energy at which the synchrotron-loss break appears decreases with age. At the highest photon energies, the steep curvature of the spectrum corresponds to the shape of the characteristic synchrotron spectrum from electrons at the uppermost end of the particle spectrum. This feature propagates downward in energy with increasing age as well. Comparison with Figure 3 makes it clear that a single magnetic field strength cannot reproduce the spectrum for both the nebula and the torus; the torus requires a break between the X-ray and infrared bands that is not seen in the

spectrum of the nebula itself. Moreover, if the low-frequency break observed in the PWN spectrum is an imprint of the injection spectrum (as in the simple models in Figure 3), the torus spectrum then requires at least two breaks beyond the IR band, one that flattens the spectrum and another that causes additional steepening. The data alone are not sufficient to constrain the position and magnitude of these breaks. More sophisticated modeling of the PWN evolution, constrained by the observed emission from the torus region, is required to understand the broadband emission.

5. CONCLUSIONS

We have presented *Spitzer* observations of 3C 58 that provide detections of the nebula at 3.6 and 4.5 μm at flux values consistent with an extrapolation of the X-ray spectrum into the mid-IR band. Moreover, our detections of the torus surrounding PSR J0205+6449 in each IRAC band, along with upper limits from *J*-band observations, show that a spectral break is required between the IR and X-ray bands, and that multiple breaks are suggested. These results show that the particles entering the nebula through the torus do not have a simple power law spectrum, and suggest that the low-frequency break in the large-scale nebula may be associated with a break in the particle spectrum injected into the nebula.

To constrain realistic evolutionary models for the structure of 3C 58 that lead to its observed spectrum, it is crucial to obtain several additional measurements for both the torus and the PWN. The position of the low frequency break for the entire nebula is currently strongly constrained by a single high-frequency measurement at ~ 100 GHz. Confirmation of this result is crucial, as are measurements of the flux in the sub-mm band. For the torus, any improvements in the radio upper limits will provide strong constraints. Just as important are longer-wavelength measurements in the IR band, and deeper measurements in the near-IR. The capabilities for each such measurement currently exist, and hold promise for expanding our understanding of not only 3C 58, but of all PWNe.

The work presented here was supported in part by *Spitzer* Grants JPL 1265776 (POS), JPL CIT 1264892 (DJH), and JPL RSA 1264893 (SPR), and as well as NASA Contract NAS8-39073 (POS).

REFERENCES

- Bietenholz, M.F. 2006, *ApJ*, 645, 1180
 Bocchino, F. et al. 2001, *A&A*, 369, 1078
 Chevalier, R. A. 2005, *ApJ*, 619, 839
 Fleishman, G. D. & Bietenholz, M. F. 2007, *MNRAS*, 376, 625
 Frail, D. A. 1998, in “The Many Faces of Neutron Stars.” Edited by R. Bucccheri, J. van Paradijs, and M. A. Alpar. Dordrecht ; Boston : Kluwer Academic Publishers, 1998., p.179
 Frail, D. A. & Moffett, D. A. 1993, *ApJ*, 408, 637
 Gotthelf, E. V., Helfand, D. J., & Newburgh, L. 2006, *ApJ*, 654, 267
 Green, D. A., & Scheuer, P. A. G. 1992, *MNRAS*, 258, 833
 Indebetouw, R. et al. 2005, *ApJ*, 619, 931
 Kennel, C.F. & Coroniti 1984, *ApJ*, 283, 710
 Murray, S. S., Slane, P. O., Seward, F. D., Ransom, S. M., & Gaensler, B. M. 2002, *ApJ*, 568, 226
 Reynolds, S. P. Proceedings of IAU Colloquium 192, 10 Years of SN1993J (Valencia, Spain, April 2003)
 Reynolds, S. P., & Aller, H. D. 1985, *AJ*, 90, 2312
 Reynolds, S. P., & Chevalier, R. A. 1984, *ApJ*, 278, 630
 Rudie, G. C., & Fesen, R. A. 2007, *RMxAC*, 30, 90
 Slane, P. et al. 2000, *ApJ*, 533, L29
 Slane, P., Helfand, D. J., & Murray, S. S. 2002, *ApJ*, 571, L45
 Slane, P., Helfand, D. J., van der Swaluw, E., & Murray, S. S. 2004, *ApJ*, 616, 403 (S04)
 Stephenson, F. R., & Green, D. A. 2005, *Historical Supernovae and Their Remnants* (Oxford University Press, USA)
 Temim, T. et al. 2006, *AJ*, 132, 1610
 Torii, K., Slane, P. O., Kinugasa, K., Hashimoto, K., & Tsunemi, H. 2000, *PASJ*, 52, 875
 van den Bergh, S. 1978, *ApJ*, 220, L9
 Woltjer, L., Salvati, M., Pacini, F., and Bandiera, R. 1997, *A&A*, 325, 295